JGR Atmospheres

RESEARCH ARTICLE
10.1029/2025JD043478

A Probabilistic Algorithm for Mitigating Persistent Ground Clutter in Doppler Weather Radar

Vaibhav Tyagi[1] and **Saurabh Das**[1]

[1]Department of Astronomy, Astrophysics and Space Engineering, Indian Institute of Technology Indore, Indore, Madhya Pradesh, India

Key Points:

- Probabilistic algorithm for ground clutter mitigation applicable to any single or dual polarized Doppler weather radar (DWR)
- Tested and evaluated using data from the TERLS C Band DWR installed at Thiruvananthapuram India
- Outperforms Gabella filter and fuzzy logic methods for persistent ground clutter removal

Correspondence to:

S. Das,
saurabh.das@iiti.ac.in;
das.saurabh01@gmail.com

Citation:

Tyagi, V., & Das, S. (2025). A probabilistic algorithm for mitigating persistent ground clutter in Doppler weather radar. *Journal of Geophysical Research: Atmospheres*, *130*, e2025JD043478. https://doi.org/10.1029/2025JD043478

Received 26 JAN 2025
Accepted 23 JUL 2025

Author Contributions:

Conceptualization: Vaibhav Tyagi, Saurabh Das
Data curation: Vaibhav Tyagi
Formal analysis: Vaibhav Tyagi
Funding acquisition: Saurabh Das
Investigation: Vaibhav Tyagi
Methodology: Vaibhav Tyagi, Saurabh Das
Resources: Saurabh Das
Supervision: Saurabh Das
Visualization: Vaibhav Tyagi
Writing – original draft: Vaibhav Tyagi
Writing – review & editing: Vaibhav Tyagi, Saurabh Das

Abstract The Doppler weather radars (DWRs) provide valuable three-dimensional (3D) information about weather systems. The presence of objects such as trees, buildings, and mountains, also known as clutter, can significantly contaminate the reflectivity echoes. In complex terrains, signal processing techniques are often inadequate in completely resolving ground clutter. This study focuses on developing an algorithm to mitigate persistent ground clutter based on long-term radar data. A composite ground clutter probability map was constructed using a texture-based approach (Gabella filter), accessing persistent ground clutter across multiple scans. Otsu's thresholding method was then applied to determine an optimal threshold that separates clutter from non-clutter regions. This results in a static binary clutter mask, which was further refined by morphological dilation. The performance of the proposed technique is evaluated on data from the C-band DWR installed at the Thumba Equatorial Rocket Launching Station (TERLS) in Thiruvananthapuram, Kerala, India. The DWR observations from January and February 2017–2024 are used, characterized by the lowest average monthly rainfall over Kerala, maximizing clear-air echoes. A total of 13,892 plan position indicator (PPI) scans (at 2-degree elevation) were considered to generate the clutter map. The quantitative analysis of the clutter removal ratio (P_{rm}) indicates that the proposed technique effectively eliminates ground clutter, achieving P_{rm} of 0.98, compared to the standalone Gabella filter ($P_{rm} = 0.54$) and fuzzy logic-based methods ($P_{rm} = 0.95$) for non-rainy cases. This method offers a practical yet simple approach to mitigating clutter in complex terrains such as the Western Ghats (WG), as demonstrated in this study.

Plain Language Summary In meteorology, Doppler weather radars (DWRs) play an important role in providing high-resolution, three-dimensional spatiotemporal measurements of various parameters of precipitation systems. The presence of objects such as trees, buildings, and mountains in the radar coverage introduces clutter signals that contaminate the reflectivity data. Clutter in general refers to the unwanted signals originating from non-meteorological targets. The present study proposed an algorithm exploiting the statistical properties of the long-term radar data. A clutter probability map is then generated using a simple texture-based approach (Gabella filter) across multiple radar volume scans. The proposed technique is demonstrated and evaluated on data from C-band DWR at the Thumba Equatorial Rocket Launching Station (TERLS) in Thiruvananthapuram, Kerala, India. The DWR data from the dry months over Kerala, that is, January and February from 2017 to 2024, is used to get the maximum number of clear-air echoes. The qualitative and quantitative analysis shows that the proposed technique significantly reduces the ground clutter compared to existing techniques, thereby enhancing the quality of DWR reflectivity data. This method offers a practical approach to mitigating clutter in complex terrain such as the Western Ghats (WG).

1. Introduction

Doppler weather radars (DWRs) are advanced active remote sensing instruments that have emerged as revolutionary instruments in meteorology. These provide continuous 3D measurements of weather systems at very high spatio-temporal resolution (Bringi & Chandrasekar, 2001; Chandrasekar et al., 2023). The DWR observations are crucial for numerous applications such as quantitative precipitation estimation (QPE), short-term weather forecasting, operational warnings, flash flood analysis, etc (Chen & Chandrasekar, 2015; Doviak & Zrnic, 2014; Doviak et al., 2000; Huong & Pathirana, 2013; Rezacova et al., 2007; Wilson et al., 1980). However, the reliability and accuracy of different applications are highly dependent on the quality of DWR data. The radar measures the backscattered power received from the targets. In the context of weather radar, the primary targets of interest are hydrometeors, that is, raindrops, cloud droplets, ice crystals, hail, etc. The echoes that do not originate from the hydrometeors are often referred to as clutter echoes. These clutter echoes can originate from various

sources. The echoes from the ground or the permanent objects, such as trees, buildings, mountains, etc., are referred to as ground clutter (Bringi & Chandrasekar, 2001). These echoes from the ground clutter are a challenging problem, especially in complex mountainous terrains, as the distribution of the ground clutter is unique and is a characteristic property of the radar site (Germann et al., 2022). These effects need to be properly mitigated as a quality control measure before working with DWR data for both qualitative and quantitative applications.

Clutter identification and mitigation are based on spectral domain characteristic features of the received radar signal from targets, which include (I) temporal stationarity, (II) near-zero mean radial velocity, (III) very narrow spectrum width, and (IV) spatial variability, such as rapid fluctuations in signal strength along range and azimuth (Rauber & Nesbitt, 2018). Usually, the ground-clutter filters (GCF) are developed based on the appropriate signal processing techniques on the received complex voltages, that is, in-phase (I) and quadrature (Q) data (Sirmans, 1987). These exploit the spectral properties to mitigate the effect of ground clutter. A notch filter-based approach removes clutter in DWR data by attenuating near-zero frequencies in the Doppler spectrum, where signals from stationary objects such as buildings and terrain dominate (Groginsky & Glover, 1980). However, it has limitations in the case of overlapping clutter and precipitation spectra. This limitation was addressed by Passarelli (1981) using an adaptive selection of notch filter parameters and signal interpolation. Moisseev and Chandrasekar (2009) proposed a technique to differentiate the clutter signal utilizing the spectral decompositions of various dual-polarized variables. The method effectively separates weather and clutter signals in the spectral domain enhancing clutter suppression in radar observations. With the advancement in technology and computational resources several algorithms have been proposed and implemented in operational systems. For instance, Ice et al. (2009) proposed an algorithm for the WSR-88D that utilizes spectral and spatial features, estimating a clutter contamination probability at each pixel. Similarly, Warde and Torres (2010) introduced an advanced automatic clutter filtering technique based on fuzzy logic for WSR-88D systems.

The advancement of radar technology with the introduction of dual-polarized capabilities has prompted researchers to explore alternative methods for ground clutter suppression. Previous studies have utilized the distinct radar signatures of various hydrometeors for hydrometeor classification using fuzzy logic techniques (Lim et al., 2005; Liu & Chandrasekar, 2000). In recent years, fuzzy logic-based techniques have emerged as a prominent alternative for clutter mitigation (Williams et al., 2009). These are based on exploiting the distinct characteristics of multiple parameters, such as reflectivity, radial velocity, spectral width, and other polarimetric variables, in differentiating different echo types. It examines the likelihood of a signal by assigning degrees of membership through a set of predefined rules. This provides the advantage of effectively handling cases with mixed signals, distinguishing clutter from weak meteorological echoes. Various studies in the past demonstrated the effectiveness of the fuzzy logic-based algorithm in differentiating the non-meteorological echoes from the precipitating echoes (Berenguer et al., 2006; Dufton & Collier, 2015; Gourley et al., 2007; Islam et al., 2012; Vulpiani et al., 2012). Researchers have also explored automated methods for identifying ground clutter using 2D plan position indicator (PPI) reflectivity scans. These approaches utilize typical clutter features such as stationarity of echoes over time, narrow spectrum width, and limited vertical extent in volume scans (Grecu & Krajewski, 2000; Steiner & Smith, 2002). These are used as input to the neural networks; however, studies suggested that even with high accuracy in the classification of reflectivity pixels, the chance of incorrect estimation of accumulated precipitation amount as compared to ground truth over a 3-hr period is 30% (Lakshmanan et al., 2007).

Another traditional way for identifying and mitigating clutter is the static clutter map, which is generated under clear-air conditions. The radar operators usually maintain such typical clutter maps that identify and eliminate the clutter before providing data to the users (Federal Meteorological Handbook, 2006; Lakshmanan et al., 2012). However, their static nature restricts adaptability to dynamic or transient clutter scenarios, such as those arising under anomalous propagation or changing weather conditions. Hernáez et al. (2012) discusses the statistical behavior of the clutter and reports that different amounts of clutter echoes were observed during cold and hot months. The evolution of clutter is associated with the effects of temperature, which creates inversion that leads to variation in clutter across different weather conditions. These limitations can be addressed by applying a fuzzy logic based dynamic filtering technique. Radar networks such as Next-Generation Radar (NEXRAD) also incorporate static clutter maps, which are complemented by dynamic clutter mitigation decisions (Hubbert et al., 2007).

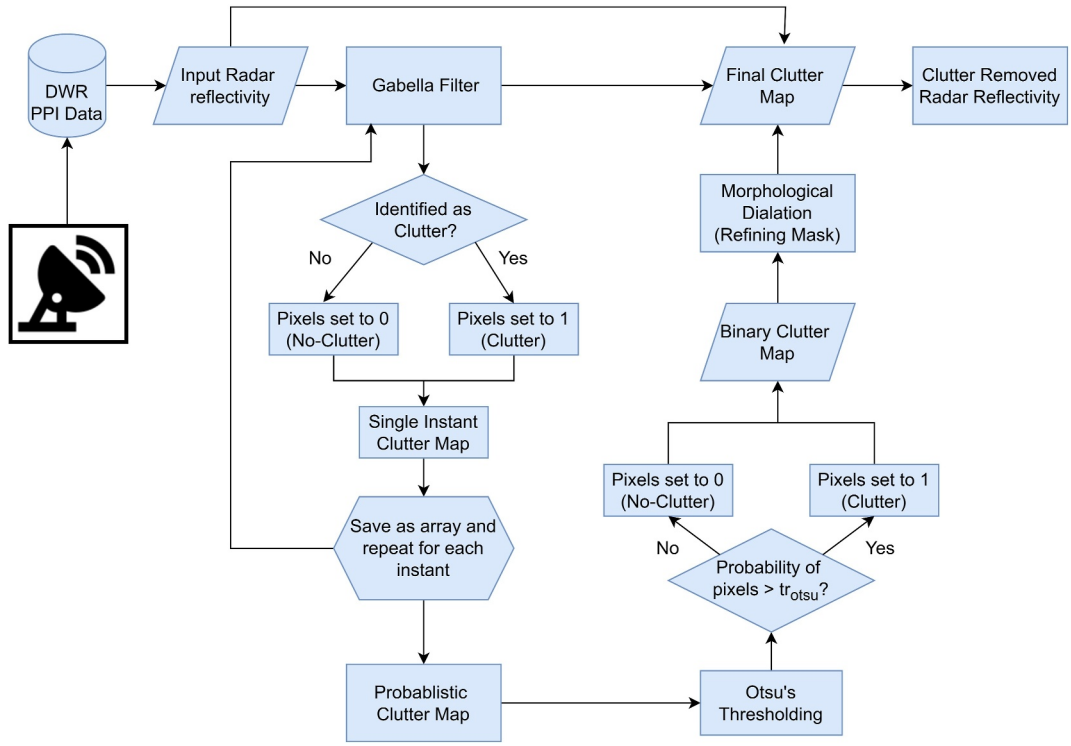

Figure 1. The flowchart representation of the proposed methodology.

The present study aims to develop an algorithm for mitigating persistent ground clutter in complex mountainous terrain by creating a probabilistic clutter map based on the statistical properties of long-term reflectivity data. Since the raw I/Q data may not be accessible to end-users, the approach utilizes only reflectivity measurements to identify clutter patterns. The study employs a texture-based algorithm proposed by Gabella and Notarpietro (2002) based on the horizontal variation of reflectivity. The long-term radar data are used to generate a probabilistic clutter map, which assigns a likelihood of clutter to each radar pixel, capturing persistent clutter. As a test case, the methodology was tested and validated on the data from a C-band DWR installed at TERLS, Thiruvananthapuram, Kerala, India. The TERLS DWR is one of the three radars maintained by the Indian Space Research Organisation (ISRO) with an open-access data policy. Its location in the complex mountain terrain of WGs makes it ideal for evaluating the proposed technique.

The paper is organized into the following sections. Section 2 provides the details of the proposed methodology. Section 3 describes the evaluation strategy and data used in the present study. Section 4 presents the results of the proposed clutter mitigation algorithm, and Section 5 presents the summary and key conclusion of the study.

2. Proposed Methodology

2.1. Ground Clutter Identification

This and subsequent sections present a strategy to identify and mitigate the ground clutter from the DWR data. A detailed flowchart outlining the methodology adapted is shown in Figure 1.

The study utilizes a texture-based algorithm to identify the residual clutter in the radar reflectivity data proposed by Gabella and Notarpietro (2002), commonly known as the Glabella filter approach. The technique has the advantage that it can be applied in both polar and Cartesian coordinate systems. Furthermore, it is a posteriori method, that is, it can be implemented after any clutter removal method. A brief description of the technique is presented below, and a more detailed discussion and the rationale behind the range of various thresholds can be found in Gabella and Notarpietro (2002). The technique is based on the horizontal spatial variation of radar reflectivity. It is divided into two parts:

- **Spatial-proximity filter:** It is based on the fact that the precipitation echoes have larger spatial continuity than ground clutter. For each pixel of interest, a 5×5 window centered around the pixel is considered. The pixel is classified as a meteorological echo if the difference between its value and that of n_p number of pixels in that window is less than a defined threshold tr_1. Otherwise, the pixel is assumed to be affected by ground clutter. The present study utilizes $n_p = 8$ and $tr_1 = 9$ dBZ, values within an acceptable range as suggested by Gabella and Notarpietro (2002).
- **Test of compactness:** The second part identifies the adjacent pixels with non-zero intensity. They are classified as the same group if they touch any eight possible directions. A ratio R is evaluated, which is the ratio of the total number of pixels in a group to the number of pixels defining its boundary. It is reported that the residual clutter has R close to 1, and choosing a threshold tr_2 slightly greater than 1 will eliminate most of the clutter Gabella and Notarpietro (2002).

A careful evaluation of the Gabella filter performance was carried out across multiple radar scans and under both rainy and non-rainy conditions (results not shown here). Analysis confirms that variations in the parameter tr_1, which is related to spatial proximity filter have a negligible impact on the filtering outcome within an acceptable range, as suggested by Gabella and Notarpietro (2002). However, the parameter tr_2 was found to be more influential. During non-rainy conditions a threshold of $tr_2 = 1.3$, effectively removed all small, isolated echoes originating from clutter-prone regions, including those near the radar blind zone. Hence, a static clutter mask was generated using non-rainy cases with $tr_2 = 1.3$ to ensure effective clutter elimination in step 1.

The clutter identification technique described above can be applied to the volumetric data with multiple sweeps in the plan position indicator (PPI) scan. For a particular sweep at a specific elevation angle, the 2D radar reflectivity field $Z(azimuth, range)$ can be used to generate a clutter map $C(azimuth, range)$, called a single instant clutter map (clutter map for individual PPI scan file).

$$C(azimuth, range) = \begin{cases} 1 & \text{if clutter is identified at } (azimuth, range) \\ 0 & \text{otherwise.} \end{cases} \quad (1)$$

2.2. Development of Probabilistic Clutter Map

In complex terrain, it was observed that the single-instance Gabella filter may not be sufficient to effectively remove ground clutter. The method is based on the assumption that precipitation echoes exhibit greater spatial continuity than ground clutter. However, in complex terrain, the terrain-induced clutter can also appear spatially coherent that leads to misclassification of clutter echoes. Hence, a probabilistic clutter map, $P(azimuth, range)$ is defined as the probability of clutter at a given pixel location $(azimuth, range)$ using all the available volume scans. The single instant clutter map (clutter map for individual PPI scan file), $C(azimuth, range)$ as defined in Equation 1 is generated using the Gabella filter. $C(azimuth, range)$ is an $n \times m$ matrix of 0 and 1 for an individual PPI scan file, which is used to generate the $P(azimuth, range)$. $P(azimuth, range)$ can be expressed as:

$$P(azimuth, range) = \frac{1}{N} \sum_{k=1}^{N} C_k(azimuth, range) \quad (2)$$

where, N is the total number of PPI scans, and $C_k(azimuth, range)$ is the clutter map generated for the k-th scan. The resulting map $P(azimuth, range)$ provides the probability of clutter being present at each pixel, with values ranging from 0 (no clutter) to 1 (clutter is highly probable).

Once the probabilistic clutter map is generated, an optimal threshold needs to be identified to create a binary clutter mask. The following section describes optimal threshold identification and binary clutter mask generation.

2.3. Optimal Threshold Identification and Binary Mask Generation

After generating a clutter probability map, the next step is to develop a binary clutter mask. This can be done by choosing an appropriate threshold to classify the clutter probability map to a binary clutter mask which identifies regions as clutter and non-clutter. Thresholding is an image segmentation technique that converts a grayscale image into a binary image by assigning pixels above a set intensity value as foreground and those below as background. This involves setting pixels to white that are above a certain threshold and black that are below it.

Threshold selection from a grayscale image is a well-studied problem (Goh et al., 2018; Sezgin & Sankur, 2004). In the context of the present study, that is, clutter classification with two classes, Otsu's thresholding is an optimal method of image segmentation into clutter and non-clutter regions. It is a global thresholding method that estimates an optimal threshold (tr_{otsu}) by maximizing the interclass variance.

Steps Involved in Otsu's Thresholding

1. **Histogram Calculation:** The normalized histogram of the probabilistic clutter map (Equation 2) is calculated, and the probability density function (PDF) is represented as $P(x)$, where $x \in [0, 1]$.
2. **Class Probabilities:** For a given threshold t, the clutter map is divided into two classes. The probabilities of the two classes are given by Equation 3.

$$w_0(t) = \int_0^t P(x)\,dx \text{ and } w_1(t) = \int_t^1 P(x)\,dx \tag{3}$$

   where, $w_o(t)$ and $w_1(t)$ represent the class probabilities of two classes, background (non-clutter) and foreground (clutter), for a given threshold t. These are calculated based on the normalized histogram of the probability clutter map.
3. **Class Means:** The means of the two classes are calculated using Equation 4.

$$\mu_0(t) = \frac{\int_0^t x \cdot P(x)\,dx}{w_0(t)} \text{ and } \mu_1(t) = \frac{\int_t^1 x \cdot P(x)\,dx}{w_1(t)} \tag{4}$$

4. **Optimal Threshold Selection:** The optimal threshold tr_{otsu} is the value that maximizes the between-class variance given by Equation 5.

$$\begin{aligned} tr_{\text{otsu}} &= \arg\max_t \sigma_B^2(t) \\ \text{where } \sigma_B^2(t) &= w_0(t) \cdot w_1(t)\big(\mu_0(t) - \mu_1(t)\big)^2 \end{aligned} \tag{5}$$

Based on the estimated optimal threshold, a binary clutter mask is generated. Let *P(azimuth, range)* represent the probability at each pixel location *(azimuth, range)*. The binary mask *M(azimuth, range)* is defined such that:

$$M(azimuth, range) = \begin{cases} 1 & \text{if } P(azimuth, range) \geq tr_{\text{otsu}} \\ 0 & \text{otherwise} \end{cases} \tag{6}$$

2.4. Morphological Operation

It is observed that there are small gaps within the binary clutter mask, thus, to refine the binary clutter mask, the morphological operation, binary dilation, is applied to the binary clutter mask generated in Equation 6. Binary dilation is a fundamental morphological operation used to refine binary masks by expanding the regions marked as foreground (i.e., pixels with a value of 1). This process is achieved by convolving the binary mask (Equation 6) with a kernel, W which defines the shape and size of the dilation window. A kernel (or structuring element) of size 3×3 is used to perform the dilation operation with only the central pixel and its immediate neighbors as one. A 3×3 kernel is chosen because it fills the small gaps within the clutter mask without overexpanding the clutter region. The dilated binary mask is mathematically expressed as:

$$M_{dilated}(azimuth, range) = \bigvee_{(i,j)\in W} M(azimuth - i, range - j) \tag{7}$$

$$W = \begin{bmatrix} 0 & 1 & 0 \\ 1 & 1 & 1 \\ 0 & 1 & 0 \end{bmatrix}$$

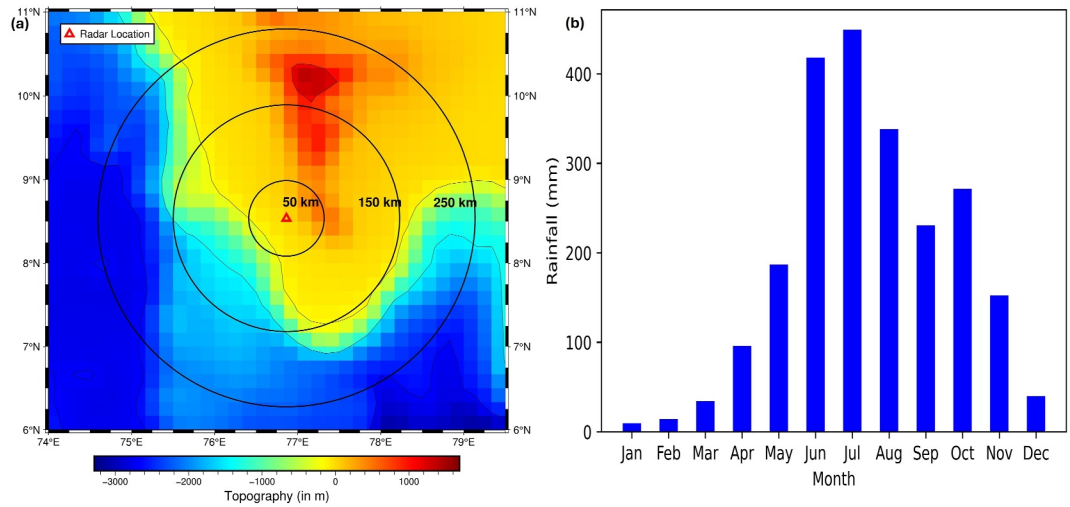

Figure 2. (a) Study map highlighting the topography of the region with a red triangle representing the location of Doppler weather radar (TERLS). The concentric rings are shown at a distance of 50, 150, and 250 km from the radar for reference. The map was created using the open-source Python library PyGMT (Uieda et al., 2021) and (b) Climatology of monthly rainfall using IMD gridded rainfall data from 1992 to 2022 over the Kerala region from 5-12 °N to 75°–77 °E.

where, W is a kernel of 3×3 size, and $\bigvee$ denotes the logical OR operation applied over the neighborhood defined by W. The dilation operation expands M such that a pixel in the output mask $M_{dilated}(azimuth, range)$ is set to 1 if any pixel in the neighborhood defined by W is 1.

After generating the final dilated clutter mask, the proposed technique first removes the persistent ground clutter from the raw reflectivity data. This is further enhanced by applying the single-instant Gabella filter to eliminate any residual clutter. In contrast to step 1, applying the same threshold during rainy conditions proved too stringent, leading to the removal of meteorological echoes even from isolated rain cells. Hence, a relaxed threshold of $tr_2 = 1.1$ was used to preserve small meteorological echoes while applying the Gabella filter in step 2. This strategy ensures a balance between clutter removal and rain echo retention.

3. Evaluation Methodology

The present study demonstrates the effectiveness of the proposed algorithm for ground clutter mitigation on a C-band DWR (latitude: 8.53°N and longitude: 76.86°E) installed at the Thumba Equatorial Rocket Launching Station (TERLS) in Thiruvananthapuram, Kerala, India. The location of the TERLS DWR (red marker) with the topography of the region is shown in Figure 2a.

3.1. Radar System and Data Set

TERLS C-band DWR is the first indigenous dual-polarized DWR in India, developed by ISRO Telemetry, Tracking and Command Network (ISTRAC). The operating frequency range of the radar is 5.6–5.65 GHz. The radar offers 360-degree azimuth and −2 to 92-degree elevation coverage with a precise beam pointing accuracy of 0.1°. It has a parabolic antenna of diameter 4.2 m with a gain of 45 dB and a pencil beamwidth of 1°. The radar system has a coherent klystron-type transmitter offering a peak power of 250 kW with a selectable pulse width of 0.5–4 μs and pulse repetition frequency (PRF) of 100–2,400 Hz. The radar supports a range resolution of 75–300 m, with up to 2,700 range bins, making it suitable for high-resolution atmospheric observations. The radar works in both single pulse repetition frequency (SPRF) and dual pulse repetition frequency (DPRF) modes and provides the data in NetCDF format. The radar system is designed to provide a range resolution of 150 m in DPRF mode and 300 m in SPRF mode, with a maximum range of 240 km in DPRF and 364.8 km in SPRF. The system supports 11 elevation angles in DPRF and three elevation angles in SPRF. The radar provides reflectivity (Z), radial velocity (V), spectrum width (σ), differential reflectivity (Z_{dr}), differential phase (ϕ_{dp}), and correlation coefficient (ρ_{hv}). A detailed description of the radar system can be found in Mishra et al. (2020). The radar data are obtained from the Meteorological & Oceanographic Satellite Data Archival Center (MOSDAC, 2016).

The present study uses the L2A (Level 2) product in DPRF mode from the TERLS C-band DWR. The L2A product provides PPI volumetric scan data at 11 elevation angles (0.5°, 1°, 2°, 3°, 4°, 7°, 9°, 12°, 15°, 18°, and 21°). The data from 2017 to 2024 for the January and February months, which are characterized by the lowest monthly rainfall are used for the present study. Over a period of 8 years from 2017 to 2024, a total of 13,892 volume scans are available. The reading and pre-processing of raw DWR data available in NetCDF format are performed using an in-house developed Python processing toolkit, PYIWR: Python Indian Weather Radar Toolkit (Singh et al., 2024).

3.2. Radar Beam Blockage Analysis

The ground clutter and its distribution are characteristic properties of the radar site and it is important to understand how the radar beam is affected by the topography. The terrain and other objects such as large buildings and trees within the radar coverage cause significant radar beam blockage (BB) (Bech et al., 2003, 2007; Germann & Joss, 2004; Joss et al., 1990). The BB fraction can be estimated using a digital elevation map (DEM) and the knowledge of the radar beam's geometry and occultation. Bech et al. (2003) proposed a geometrical-optics approach to calculate the degree of BB, given by Equation 8.

$$BB = \frac{y\sqrt{a^2 - y^2} + a^2 \arcsin\left(\frac{y}{a}\right) + \frac{\pi a^2}{2}}{\pi a^2} \tag{8}$$

where, a is the radius of the radar beam cross-section, and y is the height difference between the topography and the radar beam center. Partial beam blockage (PBB) occurs when $-a < y < a$, total blockage when $y \geq a$, and no blockage when $y \leq -a$.

The present study utilizes an open-source Python library, WRADLIB, for the partial beam blockage fraction (PBBF) calculation using Shuttle Radar Topography Mission (SRTM) data (Heistermann et al., 2013). It is important to note that the BB analysis based on the radar beam's geometry and occultation provides an estimate of potential obstruction. However, actual beam blockage can vary due to atmospheric conditions.

3.3. Comparison With Existing Methods

The performance of the proposed technique is evaluated with two widely used methods, the single-instance Gabella filter (Gabella & Notarpietro, 2002) and a fuzzy logic-based method (Vulpiani et al., 2012) to assess its robustness and efficiency. Three cases across different times of the year are presented to evaluate the performance of the clutter removal methods under varying atmospheric conditions. These cases represent distinct meteorological scenarios, including clear skies, heavy precipitation, and intense convective systems. These cases were not used in developing the clutter mask to ensure an unbiased performance assessment.

For evaluation of the performance of clutter removal techniques, frequency maps of radar reflectivity exceeding a threshold (e.g., 20 dBZ) are often used (Haibo et al., 2018; Wang et al., 2024). Haibo et al. (2018) defines a quantitative measure, a clutter removal ratio (P_{rm}), given by Equation 9.

$$P_{rm} = 1 - \frac{A_a}{A_b} \tag{9}$$

where, A_a (A_b) is the area of pixels with reflectivity greater than 20 dBZ after (before) the clutter removal. Haibo et al. (2018) found that under clear-sky conditions the (P_{rm}) is very high, close to 1, whereas for rainy conditions it is quite small.

The P_{rm} is thoroughly analyzed across multiple cases to evaluate the performance of various techniques aimed at mitigating ground clutter. Furthermore, a detailed case study is presented based on long-term radar data sets to assess the robustness and efficiency of the proposed technique in reducing ground clutter and its impact on radar-derived quantitative precipitation estimates (radar-QPE) over an extended period. The study examines the 2018 Kerala heavy rainfall event that occurred between 13 and 24 August 2018. Half-hourly rainfall data for this period are obtained from the Integrated Multi-satellitE (IMERGE) retrievals for Global Precipitation Measurement (GPM). This data set is utilized to identify the rainy and rain-free conditions. The clutter removal ratio is evaluated over the entire duration of the event to assess the effectiveness of different clutter mitigation techniques.

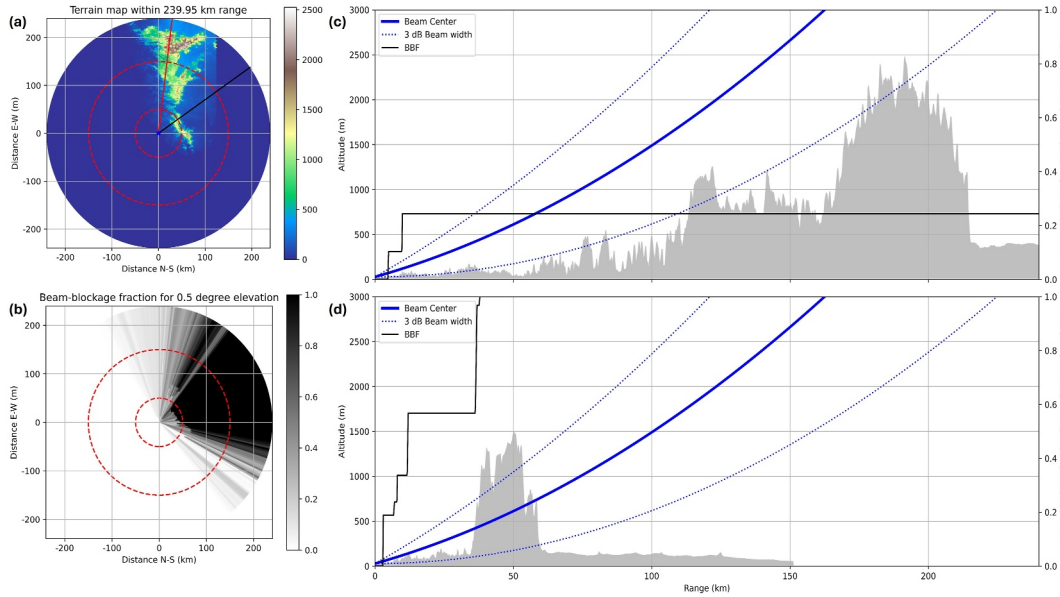

Figure 3. (a) Digital Elevation Model (DEM) depicting the regional topography using SRTM data around the Doppler weather radar site, (b) partial beam blockage fraction (PBBF) calculated for a 0.5-degree elevation angle, (c) variation of PBBF with distance from the radar overlaid with the terrain altitude along a 7-degree azimuth (red line in panel (a)), and (d) same as (c) but for a 55-degree azimuth (black line in panel (a)). The red concentric rings in panels (a) and (b) correspond to 50 and 150 km for reference.

Further, radar-QPE is analyzed to understand the impact of the clutter correction methods on rainfall retrievals. The radar rain rate is calculated from reflectivity values using a *Z-R* relationship $\left(Z = aR^b\right)$. The coefficients $a = 200$ and $b = 1.6$ are adopted from Marshall and Palmer (1948).

4. Results and Discussion

4.1. Monthly Rainfall Climatology

The India Meteorological Department (IMD) provides the daily gridded rainfall data at a grid resolution of 0.25° by 0.25°. This data set was prepared using daily rainfall data from around 6,955 rain gauge stations using the Shepard method (Pai et al., 2014; Shepard, 1968). The data set is available in NetCDF format, archived at IMD, National Data Center (NDC, 2014). The mean daily rainfall based on 31 years (1992–2022) is used to study the climatology of monthly rainfall of the region.

The averaged monthly rainfall data over the Kerala region from 5-12°N to 75-77°E is shown in Figure 2b. The monthly rainfall shows the distinct seasonal patterns driven by the Indian monsoon. The peak rainfall occurs in July (>400 mm) during the southwest monsoon phase from June to September. The southwest monsoon brings about 70%–80% of the country's annual rainfall. A secondary peak occurs in October during the northeast monsoon from October to November. In January and February, Kerala receives the least amount of monthly rainfall. These months are used for developing the clutter mask.

4.2. Radar PBB Analysis

To understand how the radar beam is affected by the topography, the beam blockage analysis is performed. Figure 3 shows the results of BB analysis for the lowest elevation angle, that is, 0.5°. The topography of the region is presented in Figure 3a, showing high elevations to the north at about 180–200 km and to the northeast of the radar at about 40–50 km. Because of these elevated terrains, the PBBF is about 1 (Figure 3b) in the northeast of the radar, as the beam is completely blocked by the WG mountains. In the north of the radar, the PBBF is about 0.2, indicating a PBB. The radar beam with topography and PBBF along 7-degree and 55-degree azimuth is shown in Figures 3c and 3d, respectively, which explains the reason for such variation of beam blockages due to the WG. It is clear from Figure 3c that the radar beam center is at about 2 km at a 120 km distance, which is well above the

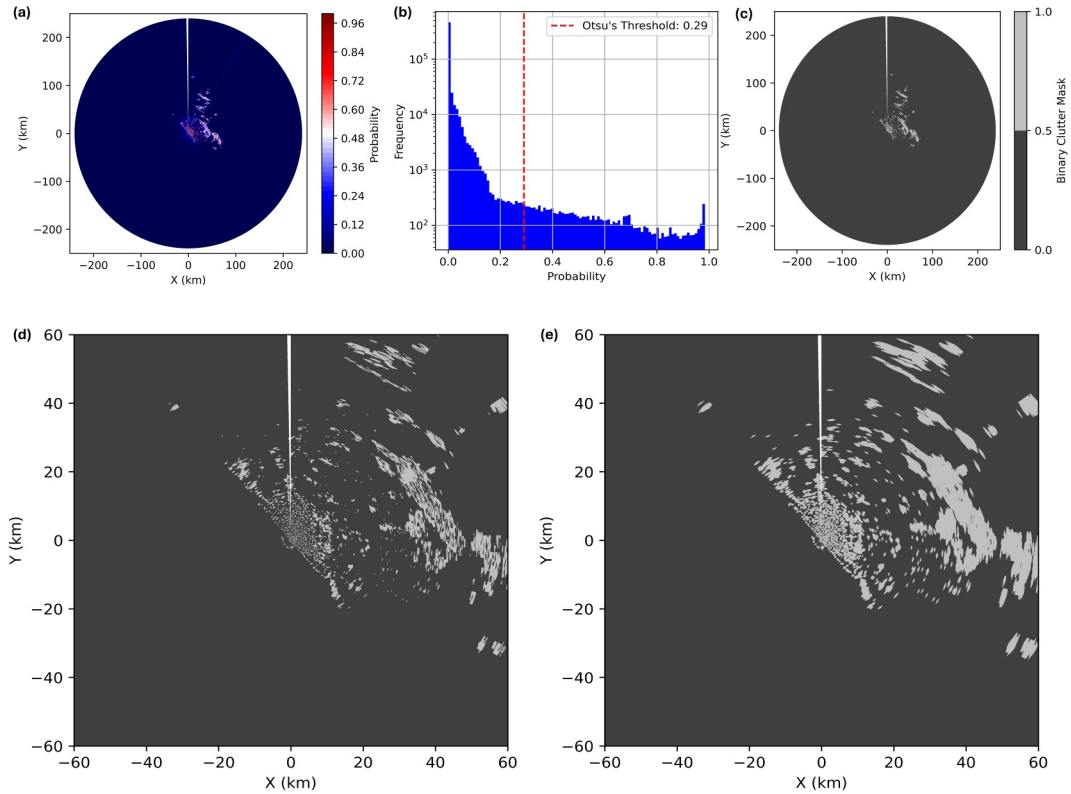

Figure 4. (a) Probabilistic clutter map for a 2-degree elevation angle, highlighting the likelihood of persistent ground clutter based on long-term reflectivity data, (b) histogram of the probabilistic clutter mask for 2-degree elevation displaying the frequency of occurrence of pixels in log-scale. The red vertical line indicates the optimal threshold determined using Otsu's thresholding technique, (c) binary clutter mask generated for the 2-degree elevation based on the threshold identified in panel (b), (d) zoomed-in view of binary clutter mask from −60 to 60 km range for 2-degree elevation, and (e) same as (d) but after morphological dilation.

height of the WGs, leading to a low PBBF of about 0.2. Although for a 55-degree azimuth, the radar beam is completely blocked by the nearby terrain, leading to PBBF equal to 1. This results in a complete blind zone in that region for the lowest elevation angle. It was observed that as compared to 0.5-degree elevation, the PBBF reduced for the higher elevation, and almost no blockage was observed in the northern region. This is because the radar beam center is well above the topography as the elevation increases.

4.3. Clutter Mask Development

The single-instance clutter maps are generated using the approach as described in Section 2. A total of 13,892 volume scans are used to generate the individual clutter maps. The analysis at 2-degree is presented and discussed in the present study. The probabilistic clutter map for a 2-degree elevation is shown in Figure 4a. It is evident from the plot that the pixels over WGs exhibit high probability values. This implies that these pixels are highly probable to be actual clutter.

Otsu's thresholding technique is then used to develop a clutter mask that classifies the pixels as clutter and non-clutter. Figure 4b shows the histogram of the clutter probability map corresponding to Figure 4a. The Otsu's threshold was found to be at 0.29, which maximizes the inter-class variance. This threshold is then used to generate the binary clutter mask. The clutter-identified pixels are highlighted in light gray, whereas the non-clutter pixels are in dark gray as shown in Figure 4c. A zoomed view of the developed clutter mask up to 60 km of the radar coverage is shown in Figure 4d. It is observed that there are small gaps within the clutter mask, as shown in Figure 4d. The morphological dilation operation is used to smooth the clutter mask by filling these small gaps, as shown in Figure 4e. Over the radar's full coverage, for a particular sweep (in this case, 2°), the total number of pixels in the clutter map is 576,000. Among these, 21,102 pixels were identified as ground clutter,

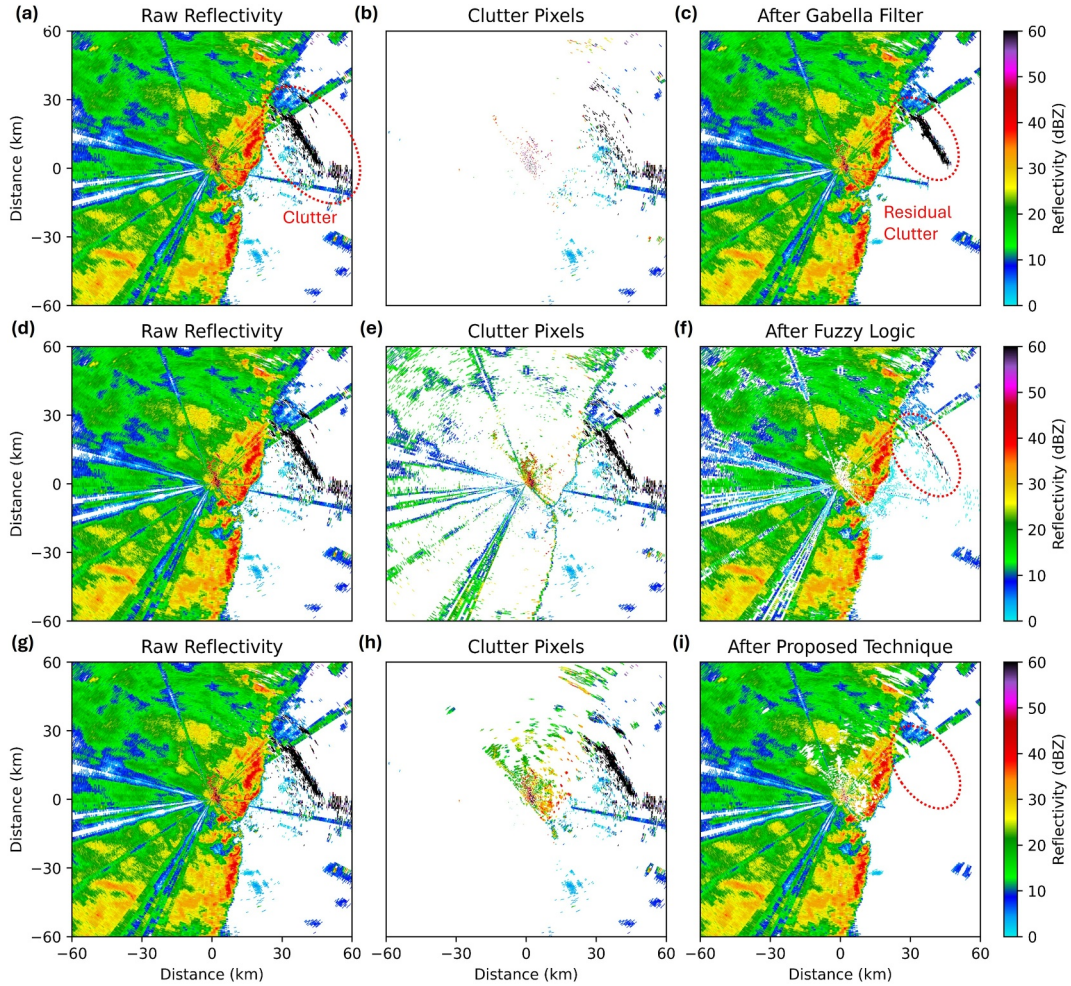

Figure 5. Radar reflectivity at 15 August 2018, 07:22:18 UTC for 2-degree elevation. The first column (a, d, and g) shows raw radar reflectivity, the second column shows clutter-removed pixels, and the third column shows corrected reflectivity after different techniques. (b, c) After Gabella filter, (e, f) fuzzy logic, and (h, i) proposed method.

which is equivalent to 3.66% of total pixels. This implies that a maximum of 21,102 pixels (3.66%) can be masked and deleted as identified as clutter after applying the clutter mask.

4.4. Performance Evaluation

In order to evaluate the performance of the clutter removal methods under varying conditions, three case studies across different times of the year are presented, along with the performance over an extended period in August 2018. Column 1 in Figures 5, 6, 7a, 7d, and 7g presents the raw radar reflectivity for 2° elevation for different timestamps, with cases representing distinct meteorological scenarios, including clear skies, heavy precipitation, and convective systems. Figure 5a corresponds to the radar reflectivity during the monsoon month on 15 August 2018 at 07:22:18 UTC. The case corresponds to a heavy rainfall event that led to widespread flooding across the state of Kerala, India. Figure 6a corresponds to the radar reflectivity for a case of a clear-air condition with no precipitation echoes. The case is from 27 January 2022 at 09:21:50 UTC. Furthermore, a third case of a pre-monsoon convective event that occurred on 18 May 2024 at 18:24:16 UTC is presented in Figure 7a. All the cases discussed above clearly show that significant ground clutter was observed to the northeast of the radar over the WG. These are the mountainous regions as shown in Figure 2a.

To assess the impact and performance of the developed clutter mask, it was compared with the single-instant Gabella filter and fuzzy logic method. Column 2 in Figures 5–7 shows the pixels removed as clutter by different techniques, whereas column 3 in Figures 5–7 shows the clutter-removed reflectivity after the

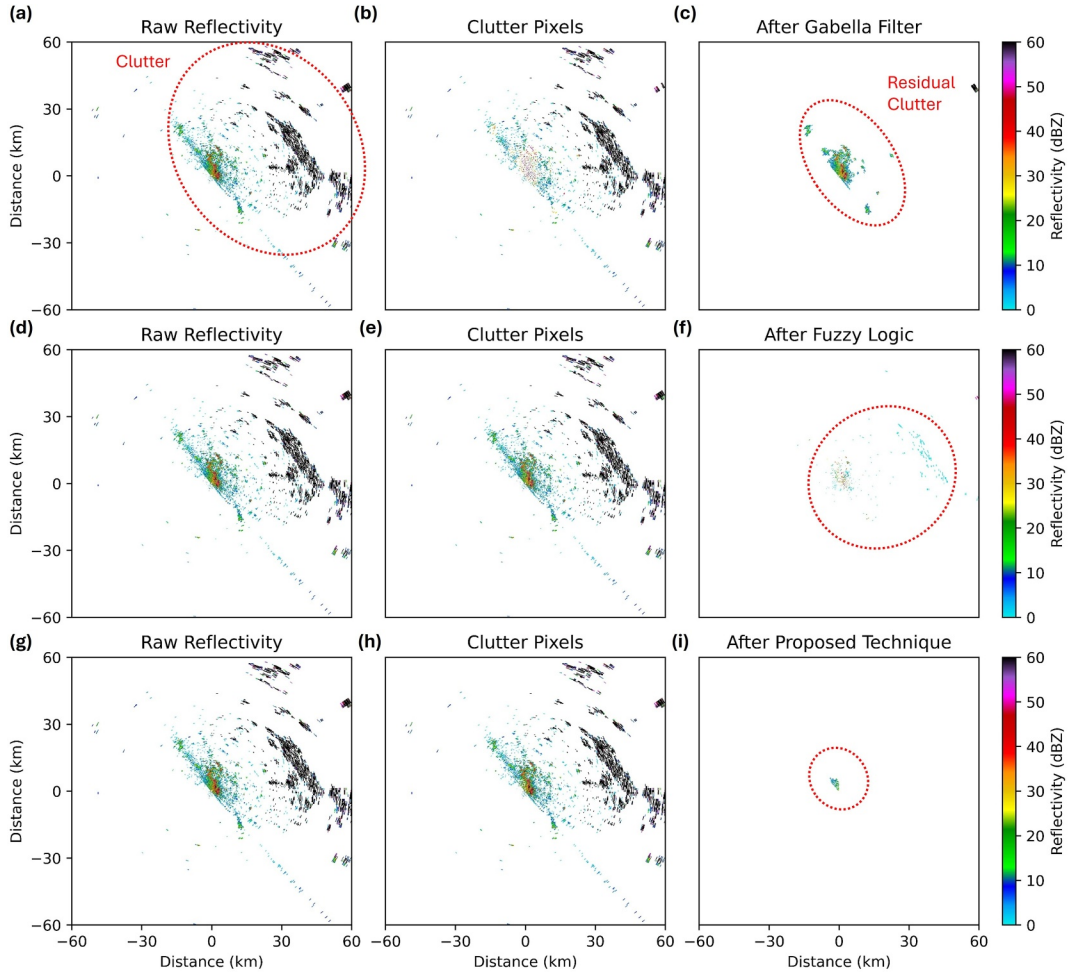

Figure 6. Radar reflectivity on 27 January 2022 at 09:21:50 UTC, for a 2-degree elevation. The first column (a, d, and g) shows raw radar reflectivity, the second column shows clutter-removed pixels, and the third column shows corrected reflectivity after different techniques. (b, c) After Gabella filter, (e, f) fuzzy logic, and (h, i) proposed method.

implementation of the Gabella filter, fuzzy logic, and proposed technique, respectively. The clutter regions before and after the correction are highlighted with red curves. Figures 5b, 5e, 5h, 6b, 6e, 6h, 7b, 7e, and 7h show the removed pixels after applying the Gabella filter, fuzzy logic, and proposed technique. It is evident from Figures 5c, 6c, and 7c that the single-instance Gabella filter failed to effectively eliminate the ground clutter observed over the WGs. Moreover, in the case of fuzzy logic, a few pixels still remained unfiltered over the WGs. However, the proposed technique successfully eliminated most of the ground clutter compared to the single-instant Gabella filter and fuzzy logic method. The fuzzy logic technique utilizes advanced dual-polarized variables, such as the correlation coefficient, to distinguish non-meteorological echoes. Consequently, it removes echoes beyond ground clutter, as evident from the differences in Figures 5e and 5h. The proposed technique, designed to specifically eliminate ground clutter, successfully eliminates most ground-clutter-affected pixels, as demonstrated in Figures 5i, 6i, and 7i. Furthermore, Figure 8 shows the normalized PDFs of the raw radar reflectivity and clutter-removed reflectivity after these three methods. Figures 8a–8c corresponds to 18 May 2024 at 18:24:16 UTC, 27 January 2022 at 09:21:50 UTC, and 15 August 2018 at 07:22:18 UTC, respectively. For all cases, a noticeable bump is observed at the tails of the PDFs at higher reflectivity values. The zoomed panel shows the probability of the pixels with such high reflectivity values. It is worth noting that the proposed technique performs better in successfully flattening the PDFs at high reflectivity values than Gabella and fuzzy logic.

We further analyzed the clutter removal ratio across these cases to quantitatively assess the performance of the proposed technique. The value of the clutter removal ratio for various cases is outlined in Table 1. It is clear that

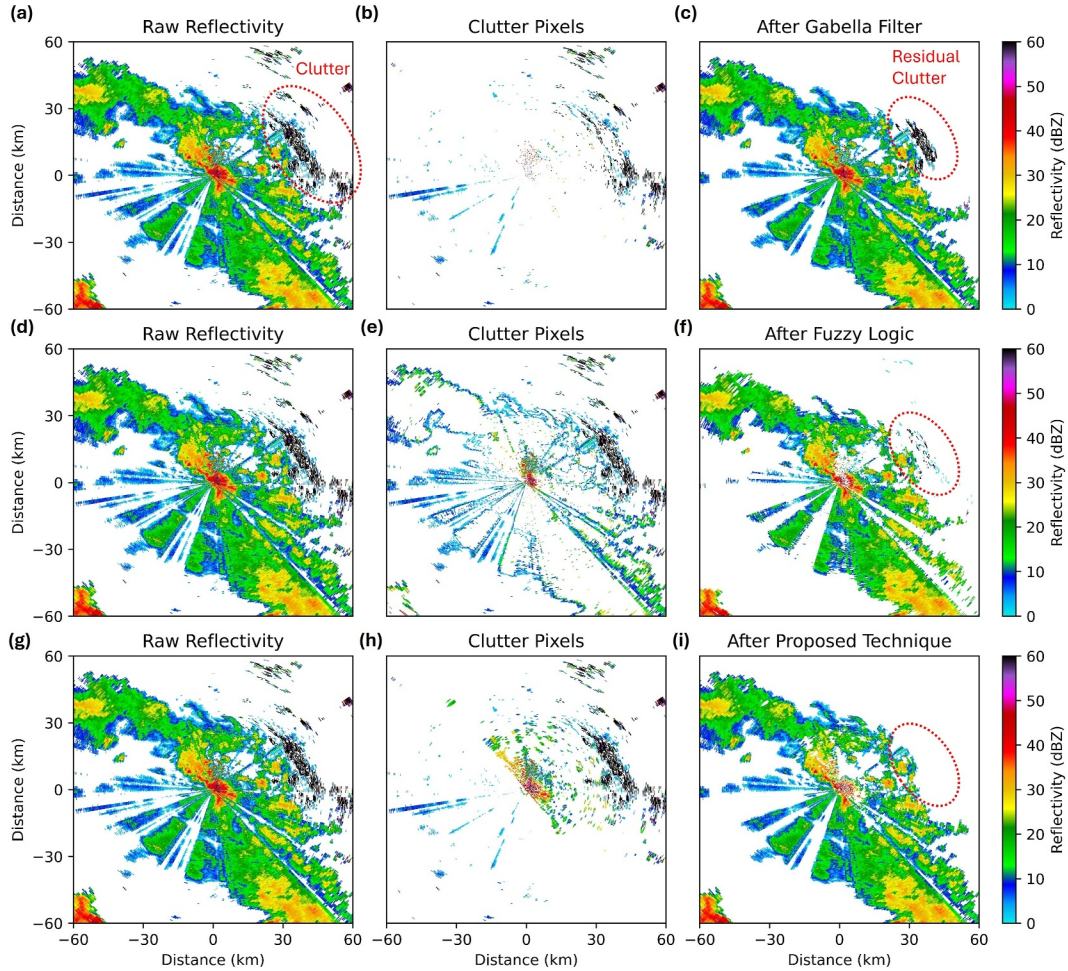

Figure 7. Radar reflectivity on 18 May 2024 at 18:24:16 UTC, for a 2-degree elevation. The first column (a, d, and g) shows raw radar reflectivity, the second column shows clutter-removed pixels, and the third column shows corrected reflectivity after different techniques. (b, c) After Gabella filter, (e, f) fuzzy logic, and (h, i) proposed method.

for the clear air echo case of 27 January 2022 at 09:21:50 UTC, the clutter removal ratio from the Gabella filter is 0.53, whereas the fuzzy logic and proposed techniques have very high removal ratios of 0.95 and 0.98, respectively. In the case of heavy precipitation and convection within the radar domain, the Gabella filter always shows a much lower value than the other two techniques. The high value in the case of clear-air echoes signifies that the proposed technique successfully removes the ground clutter. However, the low values observed in the rainy conditions indicate that there were fewer non-meteorological echoes or ground clutter echoes to remove in the first place.

4.5. 2018 Kerala Extreme Rainfall Event: A Case Study

The proposed technique shows promising results across various cases. Furthermore, a case study of the 2018 Kerala floods is presented to understand the impact of the proposed technique over an extended period. The southernmost state of India, Kerala, experienced heavy rainfall during this period which resulted in widespread flooding. The data from the TERLS C-band DWR from 13 to 23 August 2018 is used. In Figure 9, rainfall (averaged over the radar domain) is depicted by the blue curve, whereas clutter removal ratios after applying the Gabella filter, fuzzy logic, and the proposed technique are shown in red, yellow, and black, respectively. The results indicate that the clutter removal ratio from the proposed technique consistently exceeds that of the Gabella filter. During rainy conditions, the value of the removal ratio is seen to be lower. The fuzzy logic has a slightly higher clutter removal ratio than the proposed technique for the rainy case, as it eliminates other forms of clutter as

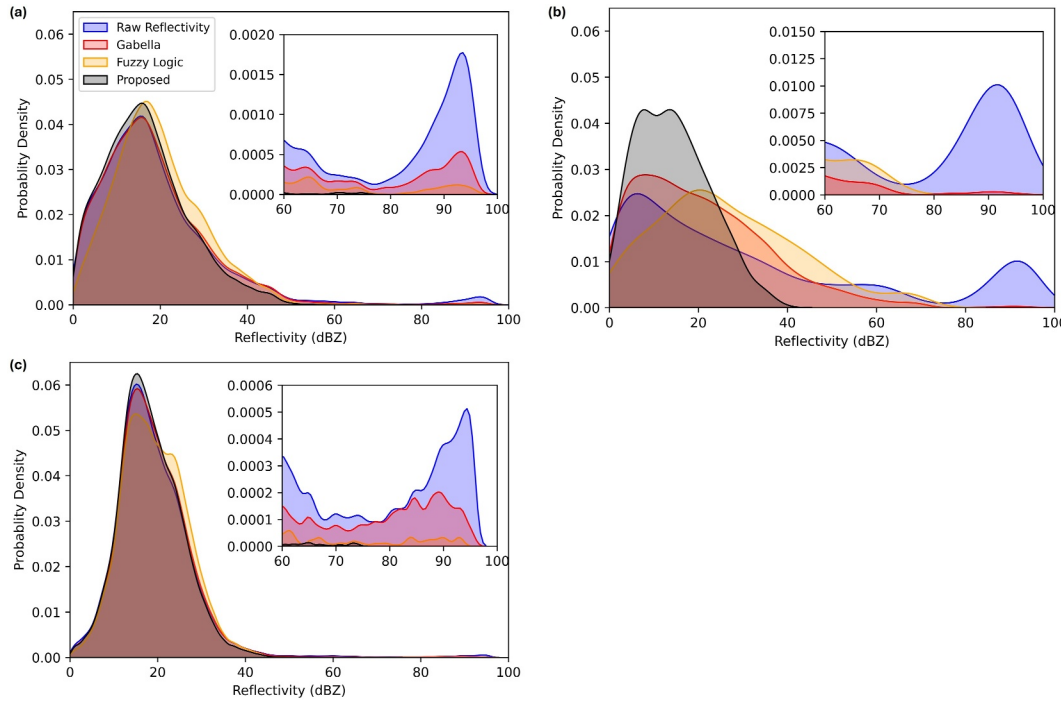

Figure 8. Normalized probability density function for raw radar reflectivity before clutter removal (blue), after Gabella filter (red), after proposed technique (black), and after fuzzy logic (yellow) for (a) 18 May 2024 at 18:24:16 UTC, (b) 27 January 2022 at 09:21:50 UTC, and (c) 15 August 2018 at 07:22:18 UTC.

well. However, from 21 to 23 August 2018, the proposed technique shows comparable performance with fuzzy logic, successfully eliminating ground clutter under near-zero rainfall conditions.

The presence of clutter significantly affects the radar-QPE. To study the impact of the proposed technique on radar-QPE, daily accumulated rainfall from the radar is compared with GPM daily accumulated rainfall averaged over the radar domain. Figure 10a shows the cumulative daily rainfall using raw radar reflectivity and clutter removal reflectivity using various techniques. For reference, the GPM daily accumulated rainfall and GPM rain rate are shown as blue and red curves, respectively. It is clear from the figure that after applying the proposed technique, the radar estimated rainfall is close to the GPM observed rainfall. However, there is a huge difference in the rainfall estimated by radar after applying the Gabella filter and fuzzy logic as compared with GPM observed rainfall. To investigate the differences in rainfall estimates by radar after applying different techniques, histograms showing the number of pixels across various rainfall bins are presented. Figures 10b and 10c show the histogram for daily accumulated rainfall for 15 August (rainy) and 23 August (near-zero rainfall) corresponding to the shaded region shown in Figure 10a. The significant difference in the two cases is that, for the case of near-zero rainfall, after applying the proposed technique, there are less pixels in higher rainfall bins. For instance, according to the Marshall-Palmer law, a reflectivity of 60 dBZ corresponds to a rain rate of approximately 205 mm/hr, whereas 80 dBZ corresponds to about 3,640 mm/hr. The presence of residual clutter pixels inflates the radar domain average rainfall, which was effectively mitigated by the proposed technique. Consequently, the proposed technique demonstrates its efficacy in eliminating persistent ground clutter and improving radar QPE estimation.

Table 1
Clutter Removal Ratio (P_{rm}) Values for Different Methods and Cases

Method	18 May 2024 18:24:16 UTC	27 January 2022 09:21:50 UTC	15 August 2018 07:20:58 UTC
Gabella filter	0.07	0.53	0.03
Fuzzy logic	0.24	0.95	0.21
Proposed technique	0.27	0.98	0.16

It is important to note that the proposed technique identifies and eliminates the clutter. Thus, this deletion of pixels may also result in the loss of some rainy pixels. An exact quantification of the same is practically challenging due to the unavailability of ground truth data as well separate resolution of DWR and GPM data. This can be handled by using appropriate interpolation techniques (if required, depending upon the application) to fill these pixels. Lakshmanan et al. (2012) discussed various strategies for correcting reflectivity data at

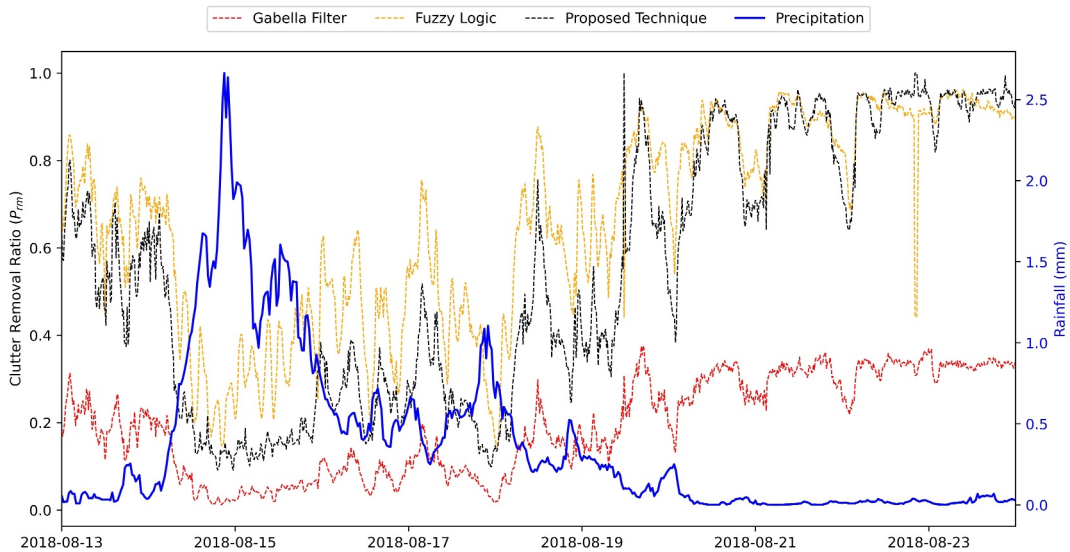

Figure 9. Variation of clutter removal ratio (P_{rm}) after different clutter removal techniques from 13 to 24 August 2018. The corresponding Global Precipitation Measurement rain rate is shown in the blue curve.

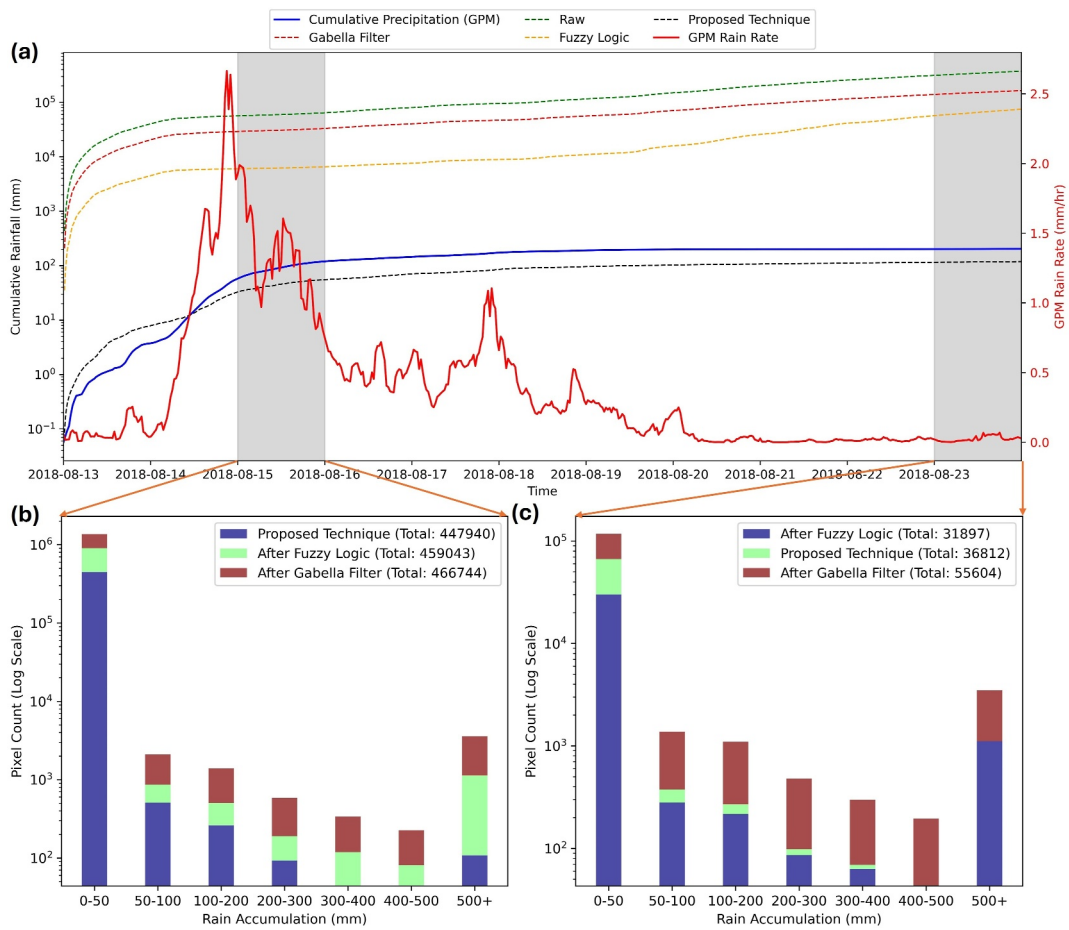

Figure 10. (a) Variation of cumulative rainfall after different techniques and from Global Precipitation Measurement (GPM) averaged over the radar domain from 13 to 24 August 2018. The corresponding GPM rain rate is shown in the red curve. Histogram of the pixels in different bins (b) for 15 August 2018, (c) for 23 August 2018.

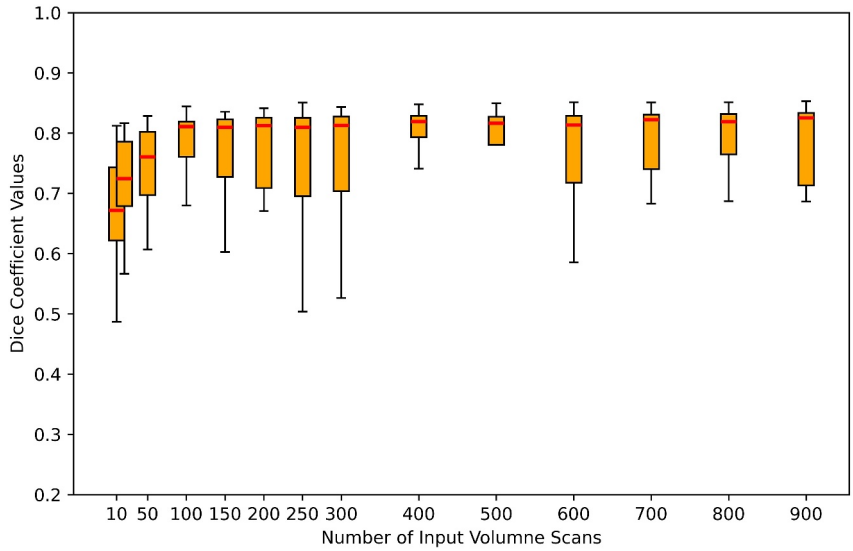

Figure 11. Variation of the Dice coefficient with the number of input volume scans used for clutter mask development.

clutter pixels, such as interpolation along radials, interpolation in 2D, etc. The same can be exercised after applying the present algorithm to fill the gaps. This is beyond the scope of the present work and can be attempted in the future.

4.6. Sensitivity Analysis

In the present study, a total of 13,892 radar scans are used to generate the clutter mask. However, the availability of such large data sets may pose a constraint. Thus, to evaluate the sensitivity of the proposed algorithm to the required input data, a sensitivity analysis is performed by varying the number of input scans used in developing the clutter mask. Different clutter masks with varying numbers of input scans (e.g., $n = 25, 50, 100\ldots$, etc.) were generated and compared with a reference clutter mask developed with all 13,892 scans. In order to quantitatively assess the similarity, a Dice coefficient is calculated. The clutter mask is generated 100 times using different random combinations of input scans to account for sampling variability. Figure 11 shows the box plot of the Dice coefficient with the number of input scans. It can be seen that the Dice coefficient reaches around 0.82 and saturates beyond $150 - 200$ input scans. It highlights that the technique is robust even with limited data and not overly dependent on the availability of a large number of input scans used to generate the clutter mask.

5. Summary and Conclusion

The echoes from the persistent ground clutter remain a critical challenge in weather radar operations, especially in regions with complex topography (Germann et al., 2022). The clutter mitigation is performed at the signal processing level itself, and for any residual clutter, appropriate post-processing techniques can be applied. Existing techniques, such as the Gabella filter, a simple texture-based approach, sometimes do not effectively eliminate the persistent ground clutter. On the other hand, techniques such as fuzzy logic usually use various dual-polarized variables to distinguish between meteorological and non-meteorological echoes. This allows the usage of this technique for dual-polarized radar. However, for the single-polarized radar, the mitigation of ground clutter is a challenging task. The present study proposed an algorithm based on a probabilistic approach to effectively handle the persistent ground clutter using the statistical properties of long-term reflectivity data. The technique implemented on the data from the C-band DWR installed at TERLS in Thiruvananthapuram, Kerala, India, demonstrated its efficacy in mitigating ground clutter in the complex terrain of WGs. The PBB analysis for the lowest elevation angle of 0.5° reveals significant blockage of the radar beam, with PBBF reaching 1 in the northeast of the radar. The partial blockage of the high-elevation radar beam by the mountainous terrain of WGs results in the observation of persistent ground clutter from that region. The proposed technique considered 13,892 volume scans to generate a probabilistic clutter mask. For a 2-degree elevation angle, a maximum of 21,102 pixels were identified as ground clutter by the static mask generated. The performance analysis, based on various case

studies as well as over an extended period, shows that the proposed technique effectively reduces persistent ground clutter, outperforming the stand-alone Gabella filter and the fuzzy logic-based method. The study also highlights the impact of the clutter removal proposed technique on radar-QPE. The radar-QPE is closely aligned with GPM observations after the implementation of the proposed technique. The proposed method uses the radar reflectivity values only, enabling its wide applicability across single and dual-polarized radar systems. It is important to note that the proposed technique deals primarily with persistent ground clutter and not all forms of clutter. Furthermore, the development of such static clutter maps also supports radar relative calibration adjustments by using ground clutter as reference static targets (Rinehart, 1978; Wolff et al., 2015).

Data Availability Statement

The IMD gridded rainfall data have been obtained from the National Data Centre (NDC) archival (https://www.imdpune.gov.in/cmpg/Griddata/Rainfall_25_NetCDF.html). The DWR data have been collected from the MOSDAC archive (www.mosdac.gov.in) and the GPM-IMERG rainfall data are obtained from NASA's Earthdata archive (https://www.earthdata.nasa.gov).

Acknowledgments
The authors acknowledge the financial support from the Oceansat-03 Utilization Program by the Space Application Center (SAC), ISRO (EOS-06 UP). One of the authors (SD) also thankfully acknowledges the financial support provided by the MoES NARM Program (MoES/16/04/2021-RDESS/NARM-4). The first author (VT) thankfully acknowledges the University Grant Commission (UGC) for providing financial support as a Ph.D. fellowship (231610080045). The authors thank the India Meteorology Department (IMD), India, for providing the daily rainfall data and the team of the Meteorological & Oceanographic Satellite Data Archival Center (MOSDAC) for providing the TERLS DWR data. The authors are thankful to NASA's Earthdata portal team for providing GPM-IMERG rainfall data. The authors are also thankful to the two anonymous reviewers for their valuable comments and suggestions.

References

Bech, J., Codina, B., Lorente, J., & Bebbington, D. (2003). The sensitivity of single polarization weather radar beam blockage correction to variability in the vertical refractivity gradient. *Journal of Atmospheric and Oceanic Technology*, *20*(6), 845–855. https://doi.org/10.1175/1520-0426(2003)020<0845:tsospw>2.0.co;2

Bech, J., Gjertsen, U., & Haase, G. (2007). Modelling weather radar beam propagation and topographical blockage at northern high latitudes. *Quarterly Journal of the Royal Meteorological Society: A Journal of the Atmospheric Sciences, Applied Meteorology and Physical Oceanography*, *133*(626), 1191–1204. https://doi.org/10.1002/qj.98

Berenguer, M., Paredes, D., Llasat, M. C., & Soria, J. M. (2006). Improvement of radar precipitation estimates in orographic regions using fuzzy logic and its application to the Catalan coast. *Atmospheric Research*, *79*, 291–302.

Bringi, V., & Chandrasekar, V. (2001). *Polarimetric Doppler weather radar: Principles and applications*. Cambridge University Press.

Chandrasekar, V., Beauchamp, R. M., & Bechini, R. (2023). *Introduction to dual polarization weather radar: Fundamentals, applications, and networks*. Cambridge University Press.

Chen, H., & Chandrasekar, V. (2015). The quantitative precipitation estimation system for Dallas–Fort Worth (DFW) urban remote sensing network. *Journal of Hydrology*, *531*, 259–271. https://doi.org/10.1016/j.jhydrol.2015.05.040

Doviak, R. J., Bringi, V., Ryzhkov, A., Zahrai, A., & Zrnić, D. (2000). Considerations for polarimetric upgrades to operational WSR-88D radars. *Journal of Atmospheric and Oceanic Technology*, *17*(3), 257–278. https://doi.org/10.1175/1520-0426(2000)017<0257:cfputo>2.0.co;2

Doviak, R. J., & Zrnic, D. S. (2014). *Doppler radar & weather observations*. Academic Press.

Dufton, D., & Collier, C. (2015). Fuzzy logic filtering of radar reflectivity to remove non-meteorological echoes using dual polarization radar moments. *Atmospheric Measurement Techniques*, *8*(10), 3985–4000. https://doi.org/10.5194/amt-8-3985-2015

Federal Meteorological Handbook. (2006). Doppler radar meteorological observations: Part C—WSR-88D products and algorithms (Technical Report No. FCM-H11C-2006).

Gabella, M., & Notarpietro, R. (2002). Ground clutter characterization and elimination in mountainous terrain. In *Proceedings of ERAD* (Vol. 305).

Germann, U., Boscacci, M., Clementi, L., Gabella, M., Hering, A., Sartori, M., et al. (2022). Weather radar in complex orography. *Remote Sensing*, *14*(3), 503. https://doi.org/10.3390/rs14030503

Germann, U., & Joss, J. (2004). Operational measurement of precipitation in mountainous terrain. In *Weather radar: Principles and advanced applications* (pp. 52–77). Springer.

Goh, T. Y., Basah, S. N., Yazid, H., Safar, M. J. A., & Saad, F. S. A. (2018). Performance analysis of image thresholding: Otsu technique. *Measurement*, *114*, 298–307. https://doi.org/10.1016/j.measurement.2017.09.052

Gourley, J. J., Tabary, P., & Parent du Chatelet, J. (2007). A fuzzy logic algorithm for the separation of precipitating from nonprecipitating echoes using polarimetric radar observations. *Journal of Atmospheric and Oceanic Technology*, *24*(8), 1439–1451. https://doi.org/10.1175/jtech2035.1

Grecu, M., & Krajewski, W. F. (2000). An efficient methodology for detection of anomalous propagation echoes in radar reflectivity data using neural networks. *Journal of Atmospheric and Oceanic Technology*, *17*(2), 121–129. https://doi.org/10.1175/1520-0426(2000)017<0121:aemfdo>2.0.co;2

Groginsky, H. L., & Glover, K. M. (1980). Weather radar canceller design. In *19th Conference on Radar Meteorology* (pp. 192–198).

Haibo, Z., Zhang, S., Liang, X., & Xueting, Y. (2018). Improved algorithms for removing isolated non-meteorological echoes and ground clutters in CINRAD. *Journal of Meteorological Research*, *32*(4), 584–597. https://doi.org/10.1007/s13351-018-7176-9

Heistermann, M., Jacobi, S., & Pfaff, T. (2013). An open source library for processing weather radar data (*wradlib*). *Hydrology and Earth System Sciences*, *17*(2), 863–871. https://doi.org/10.5194/hess-17-863-2013

Hernáez, I., Maruri, M., & López, J. (2012). Adaptive clutter filtering using statistical radar data and atmospheric propagation conditions. In *Proceedings of ERAD*.

Hubbert, J., Dixon, M., & Kessinger, C. (2007). Real time clutter identification and mitigation for NEXRAD. In *23rd conference on interactive information processing systems*.

Huong, H. T. L., & Pathirana, A. (2013). Urbanization and climate change impacts on future urban flooding in Can Tho city, Vietnam. *Hydrology and Earth System Sciences*, *17*(1), 379–394. https://doi.org/10.5194/hess-17-379-2013

Ice, R. L., Rhoton, R., Krause, J., Saxion, D., Boydstun, O., Heck, A., et al. (2009). Automatic clutter mitigation in the WSR-88D, design, evaluation, and implementation. In *34th conference on radar meteorology, Williamsburg, VA* (Vol. 93).

Islam, T., Rico-Ramirez, M. A., Han, D., & Srivastava, P. K. (2012). Artificial intelligence techniques for clutter identification with polarimetric radar signatures. *Atmospheric Research*, *109*, 95–113. https://doi.org/10.1016/j.atmosres.2012.02.007

Joss, J., Waldvogel, A., & Collier, C. (1990). Precipitation measurement and hydrology. In *Radar in Meteorology: Battan Memorial and 40th Anniversary Radar Meteorology Conference* (pp. 577–606).

Lakshmanan, V., Fritz, A., Smith, T., Hondl, K., & Stumpf, G. (2007). An automated technique to quality control radar reflectivity data. *Journal of Applied Meteorology and Climatology*, *46*(3), 288–305. https://doi.org/10.1175/jam2460.1

Lakshmanan, V., Zhang, J., Hondl, K., & Langston, C. (2012). A statistical approach to mitigating persistent clutter in radar reflectivity data. *IEEE Journal of Selected Topics in Applied Earth Observations and Remote Sensing*, *5*(2), 652–662. https://doi.org/10.1109/jstars.2011.2181828

Lim, S., Chandrasekar, V., & Bringi, V. N. (2005). Hydrometeor classification system using dual-polarization radar measurements: Model improvements and in situ verification. *IEEE Transactions on Geoscience and Remote Sensing*, *43*(4), 792–801. https://doi.org/10.1109/tgrs.2004.843077

Liu, H., & Chandrasekar, V. (2000). Classification of hydrometeors based on polarimetric radar measurements: Development of fuzzy logic and neuro-fuzzy systems, and in situ verification. *Journal of Atmospheric and Oceanic Technology*, *17*(2), 140–164. https://doi.org/10.1175/1520-0426(2000)017<0140:cohbop>2.0.co;2

Marshall, J. S., & Palmer, W. M. K. (1948). The distribution of raindrops with size. *Journal of the Atmospheric Sciences*, *5*(4), 165–166.

Mishra, S., Shanmuga Sundari, J., Channabasava, B., & Anandan, V. (2020). First indigenously developed polarimetric C-band Doppler weather radar in India and its first hand validation results. *Journal of Electromagnetic Waves and Applications*, *34*(6), 825–840. https://doi.org/10.1080/09205071.2020.1742798

Moisseev, D. N., & Chandrasekar, V. (2009). Polarimetric spectral filter for adaptive clutter and noise suppression. *Journal of Atmospheric and Oceanic Technology*, *26*(2), 215–228. https://doi.org/10.1175/2008jtecha1119.1

MOSDAC. (2016). Meteorological & oceanographic satellite Data Archival Centre (MOSDAC) [Dataset]. *Space Applications Centre (SAC), Indian Space Research Organisation*. Retrieved from https://www.mosdac.gov.in

NDC. (2014). IMD yearly gridded rainfall [Dataset]. *National Data Centre (NDC)*. Retrieved from https://www.imdpune.gov.in/cmpg/Griddata/Rainfall_25_NetCDF.html

Pai, D., Rajeevan, M., Sreejith, O., Mukhopadhyay, B., & Satbha, N. (2014). Development of a new high spatial resolution 0.25 × 0.25 long period (1901-2010) daily gridded rainfall data set over India and its comparison with existing data sets over the region. *Mausam*, *65*(1), 1–18. https://doi.org/10.54302/mausam.v65i1.851

Passarelli, R. (1981). Ground clutter rejection in the frequency domain. In *Proceedings of 20th conference on radar meteorology, Boston* (Vol. 1981). American Meteorological Society.

Rauber, R. M., & Nesbitt, S. W. (2018). *Radar meteorology: A first course*. John Wiley & Sons.

Rezacova, D., Sokol, Z., & Pesice, P. (2007). A radar-based verification of precipitation forecast for local convective storms. *Atmospheric Research*, *83*(2–4), 211–224. https://doi.org/10.1016/j.atmosres.2005.08.011

Rinehart, R. (1978). On the use of ground return targets for radar reflectivity factor calibration checks. *Journal of Applied Meteorology*, *17*(9), 1342–1350. https://doi.org/10.1175/1520-0450(1978)017<1342:otuogr>2.0.co;2

Sezgin, M., & Sankur, B. l. (2004). Survey over image thresholding techniques and quantitative performance evaluation. *Journal of Electronic Imaging*, *13*(1), 146–168. https://doi.org/10.1117/1.1631315

Shepard, D. (1968). A two-dimensional interpolation function for irregularly-spaced data. In *Proceedings of the 1968 23rd ACM National Conference* (pp. 517–524).

Singh, N., Tyagi, V., Das, S., Sahoo, U. K., & Kundu, S. S. (2024). Python Indian Weather Radar Toolkit (pyiwr): An open-source Python library for processing, analyzing and visualizing weather radar data. *Journal of Computational Science*, *81*, 102363. https://doi.org/10.1016/j.jocs.2024.102363

Sirmans, D. (1987). NEXRAD suppression of land clutter echo due to anomalous microwave propagation—Part 1 [Technical Report].

Steiner, M., & Smith, J. A. (2002). Use of three-dimensional reflectivity structure for automated detection and removal of nonprecipitating echoes in radar data. *Journal of Atmospheric and Oceanic Technology*, *19*(5), 673–686. https://doi.org/10.1175/1520-0426(2002)019<0673:uotdrs>2.0.co;2

Uieda, L., Tian, D., Leong, W. J., Toney, L., Schlitzer, W., Grund, M., et al. (2021). PyGMT: A python interface for the generic mapping tools. *Zenodo*.

Vulpiani, G., Montopoli, M., Passeri, L. D., Gioia, A. G., Giordano, P., & Marzano, F. S. (2012). On the use of dual-polarized C-band radar for operational rainfall retrieval in mountainous areas. *Journal of Applied Meteorology and Climatology*, *51*(2), 405–425. https://doi.org/10.1175/jamc-d-10-05024.1

Wang, J., Zou, H., Zhong, L., & Hu, Z. (2024). Recognition of ground clutter in single-polarization radar based on gated recurrent unit. *Remote Sensing*, *16*(23), 4609. https://doi.org/10.3390/rs16234609

Warde, D., & Torres, S. (2010). A novel ground-clutter-contamination mitigation solution for the NEXRAD network: The CLEAN-AP filter. In *Preprints, 26th conference on interactive Information and Processing Systems (IIPS) for meteorology, oceanography, and hydrology, Atlanta, GA* (Vol. 8). American Meteorological Society.

Williams, J. K., Kessinger, C., Abernethy, J., Kessinger, C., & Ellis, S. (2009). Fuzzy logic applications. In *Artificial intelligence methods in the environmental sciences* (pp. 347–377). Springer.

Wilson, J., Carbone, R., Baynton, H., & Serafin, R. (1980). Operational application of meteorological Doppler radar. *Bulletin of the American Meteorological Society*, *61*(10), 1154–1168. https://doi.org/10.1175/1520-0477(1980)061<1154:oaomdr>2.0.co;2

Wolff, D. B., Marks, D. A., & Petersen, W. A. (2015). General application of the relative calibration adjustment (RCA) technique for monitoring and correcting radar reflectivity calibration. *Journal of Atmospheric and Oceanic Technology*, *32*(3), 496–506. https://doi.org/10.1175/jtech-d-13-00185.1